33rd Annual International Conference of the IEEE EMBS
Boston, Massachusetts USA, August 30 - September 3, 2011

Computational Modeling to Evaluate Helical Electrode Designs

Anthony W. Cowley and Robert B. Szlavik

Abstract—**Finite element models of helical electrodes were utilized in conjunction with nerve fiber models to determine the efficacy of various changes in helical electrode design in improving nerve fiber recruitment. It was determined that an increase in the helical overlap angle does not facilitate recruitment of smaller diameter nerve fibers. The simulations led to some strategies that could potentially improve the electrode design.**

I. Introduction

THE use of single conductor helical electrodes is common in peripheral nerve stimulation applications that require maximal or near-maximal stimulation of a nerve trunk. Commercially, the Vagus Nerve Stimulation Therapy system (Cyberonics, Inc.) uses two helical electrodes for bipolar stimulation to treat refractory epilepsy and depression.

There have been several studies related to the safety of helical electrodes. Some of these studies attempt to predict or measure nerve damage due to mechanical pressure of the electrode and injury caused during implantation. Other studies investigated damage caused by electrical stimulation using helical electrodes [1]. There has been little work done, however, to characterize the nerve fiber excitation pattern created by such electrodes. A thorough understanding of the electric potential created within the nerve and its effect on nerve fiber stimulation may help identify shortcomings in current helical electrode designs, and also suggest possible design improvements.

II. Methods

A. Finite Element Models

In order to investigate the effects of electrode design changes on fiber activation within a nerve, a two part model was created. The model consisted of an FEA part used to calculate the electric potential within the nerve, and a nerve fiber model to determine fiber activation. A simplified vagus nerve was created, similar to the geometry used by Choi, et al. [2]. The 8 cm long nerve model had a diameter of 1.8 mm and contained several internal features including six 0.36 mm diameter fascicles with a 0.03 mm layer of perineurium surrounding each. Other features of the model included an epineurium between the fascicles and a 0.115 mm layer of connective tissue surrounding the nerve. Models of two 2mm VNS electrodes were placed around the nerve. The ANSYS Version 11.0 finite element package was used to calculate the electric potential within the modeled vagus nerve, for each of the modeled electrodes. Because the pulse widths investigated were sufficiently long (250 μs), and the capacitive effect of biological tissue is very small (less than 10% [3]), steady state FEA models were used [4]. A cylindrical domain with a radius of 6 cm was created around the nerve and electrodes to represent the surrounding tissue and fluid. A zero volt boundary condition was applied to the outside surfaces of the cylindrical domain, a negative electric current load (-2.5 mA) was applied to the face of the cathode, and a positive load (2.5 mA) to the anode. The tissue conductivities used can be found in Table 2 below where the perineurium conductivity was calculated from Frieswijk *et al* [5]. The conductivity of the helical was chosen to approximate a perfect insulator. Due to the thin internal structures within the modeled nerve, 2D elements were created on one end of the nerve and swept along the length of the nerve, while the domain and helices were meshed with tetrahedral elements. Quadrilateral to tetrahedral transitional elements were used in the connective tissue region to interface between the two different element geometries.

Material	Conductivity (S/m)	Source
Epineurium	0.008	[6]
Perineurium	0.0023	[5-6]
Fascicle – Axial	0.5	[7]
Fascicle – Radial	0.08	[7]
Surrounding Tissue	0.2	[6]
Connective Tissue (Chronic Implant)	0.16667	[3]
Helical	$1 \cdot 10^{-17}$	

Table 1: Conductivities used in finite element models.

B. Linear Nerve Fiber Model

A linear cable model, similar to that presented by Warman, *et al.* [8] was constructed to investigate the locations and fiber diameters being stimulated. The model assumes that the myelin between nodes is a perfect insulator [7]. Figure 1 shows an equivalent circuit model overlaid on a representation of an axial cross-section of nerve fiber. The transmembrane conductances were assumed to be constant until the activation threshold is reached. This assumption greatly simplifies the determination of fiber activation and is generally considered valid. It is especially useful in cases

Manuscript received April 15, 2011. This work was supported in part by Cyberonics, Inc.

A. W. Cowley was with California Polytechnic State University, San Luis Obispo, CA 93407. He is now with Cyberonics, Inc. Houston, TX 77058 USA Phone: 805-550-7162; e-mail: acowley@cyberonics.com).

R. B. Szlavik, is with California Polytechnic State University, San Luis Obispo, CA 93407 USA (e-mail: rszlavik@calpoly.edu).

where determining the excitation of a large number of fibers is required [9,10] because the computational cost is much lower than in a non-linear fiber model with time and voltage dependent membrane conductances.

Symbol	Description
D	Fiber diameter
d	Axon diameter
l	Length of Node of Ranvier
R_m	Membrane resistance
R_a	Axoplasm resistance
C_m	Membrane capacitance
L	Internodal length
$V_e(n,t)$	Time dependent extracellular voltage at node n
$V_i(n,t)$	Time dependent intracellular voltage at node n
$V_m(n,t)$	Time dependent transmembrane potential at node n
V_r	Membrane resting potential
$I_i(n,t)$	Intracellularly injected current at node n

Table 2. Symbols used in nerve fiber model

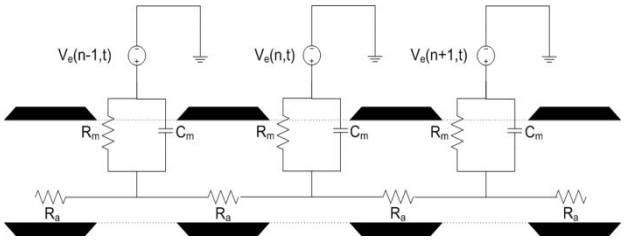

Fig 1. Equivalent circuit model of a nerve fiber.

Kirchhoff's current law can be written at each of the intracellular nodes in Figure 1 above. Note that V_m, the transmembrane potential, V_i, the internal cell potential, V_e, the external cell potential, and V_r, the resting cellular potential are related by Equation (4), and also that the cell conductances G_a and G_m are the inverses of the resistances of R_a and R_m, respectively. Writing KCL at node n and rearranging yields Equation (1)

$$\begin{aligned} &C_m \frac{dV_m(n,t)}{dt} + G_m V_m(n,t) - \\ &G_a[V_m(n-1,t) - 2V_m(n,t) + V_m(n+1,t)] \\ &= G_a[V_e(n-1,t) - 2V_e(n,t) + V_e(n+1,t)] \end{aligned} \quad (1)$$

In order to simplify the analysis, it can readily be shown that the extracellular potentials, $V_e(n,t)$ can be replaced by intracellular current sources. These current sources must be equivalent to the current on the right hand side of Equation (1) above. This is sometimes called the activating function, as it determines the current flowing into the neuron. It can be seen from Equation (3) that the intracellular current sources are dependent on the second spatial difference of the extracellular potential between adjacent nodes.

$$\begin{aligned} &C_m \frac{dV_m(n,t)}{dt} + G_m V_m(n,t) - G_a[V_m(n-1,t) \\ &-2V_m(n,t) + V_m(n+1,t)] = I_i(n,t) \end{aligned} \quad (2)$$

$$I_i(n,t) = G_a[V_e(n-1,t) - 2V_e(n,t) + V_e(n+1,t)] \quad (3)$$

$$V_m(n,t) = V_i(n,t) - V_e(n,t) - V_r(n,t) \quad (4)$$

Two centimeter sections of neuron were simulated at various locations within the nerve, with diameters ranging from 20 μm to 1 μm. Because nodal and internodal length is dependent upon diameter, the number of nodes varied from 31, in the largest fibers, to 149 in the smallest. The cell parameters G_m, G_a, and C_m are also dependent on the cell dimensions and can be readily calculated from the equations and published data listed. The solution to the FEA models gives a scalar potential value at discrete points within the volume. The extracellular potential is found by averaging the potential at the nearest points around each Node of Ranvier. This potential is then translated to an intracellularly injected current by Equation (3) which is applied to the fiber for a time equal to the specified pulse width of 250 μs.

$$G_a = \frac{\pi d^2}{4\rho_a L} \quad (5)$$

$$G_m = \pi l d g_m \quad (6)$$

$$C_m = \pi l d c_m \quad (7)$$

In all of the modeled electrodes, 66 nerve locations were examined, 11 per fascicle. It is assumed that the fibers are aligned axially with the nerve. Several fiber diameters (1-20 μm) were tested at each location in order to determine the smallest fiber activated at each location. A threshold value of 25 mV was used to delineate excitation [8, 10]. That is, if the transmembrane potential at any node increased to 25 mV above its resting potential (V_r) during the time course of the pulse, the program recorded that this fiber had depolarized sufficiently to generate an action potential.

Two sets of finite element models were created to investigate two specific design changes. In the first set, the length of the conductive electrode ribbon was varied to wrap around the nerve between 270° and 720°, while all other dimensions were held constant. The second set of models also varied the length of the electrode ribbon, but the surface area was held constant by varying the width of the ribbon.

In order to investigate the effect of the circumferential electrode coverage on nerve stimulation, models were created with varying electrode lengths, from $\theta = 270°$ to $\theta = 720°$. In all, 31 models were created with an incremental increase in coverage of $\Delta\theta = 15°$. All other dimensions of

the nerve and helical were held constant. For all of the FEA models, a 2.5 mA current was applied to one electrode, and -2.5 mA to the other. Table 3 shows the average minimum diameter fiber stimulated for some of the modeled θ values. It also shows the results of a t-test for these values against the original length of θ = 270°.

III. Results

The results from these models showed no significant decline in the mean values of the smallest fiber stimulated at electrode lengths beyond θ = 360°. It can be seen from the graphs that the overlapping electrode did not result in any increase in stimulation of smaller diameter fibers. In fact, the overlap greatly decreased stimulation. Individual nerve fibers near the area of radial electrode overlap showed a lower peak voltage and the change in voltage is more gradual, which results in a lower current injected into the cell. Examination of the individual models in Figures 2 and 3 shows that the excitation pattern is not uniform. Fewer small diameter fibers are stimulated near the electrode ends in all of the models. This area of decreased stimulation grows larger as the electrode is extended beyond θ = 360°.

	Constant Width Electrode		Narrowed Electrode	
Θ	**Mean Fiber (μm)**	**t-test p-value**	**Mean Fiber (μm)**	**t-test p-value**
270	1.6591		1.6591	
285	1.6591	1	1.5833	0.008033
300	1.6591	1	1.5682	0.000927
315	1.6515	0.791231	1.5758	0.001263
330	1.6288	0.267952	1.5909	0.038189
345	1.5985	0.016681	1.6212	0.384523
360	1.5833	0.001682	1.6742	0.78192
375	1.6667	0.882417	1.7197	0.34706
390	1.7197	0.325649	1.7197	0.34706
405	1.7803	0.084712	1.7424	0.198104
420	1.7803	0.084712	1.7803	0.084712

Table 3: The average smallest fiber stimulated for several electrode configurations and 2 sample t-test p-values comparing each to a 270° electrode.

The other set of models held the surface area of the electrode constant, while increasing the length. The electrode was narrowed by a factor equal to that of the increase in length. The applied current was again 2.5 mA and -2.5 mA, and the pulse width for the nerve fiber model was 250 μs. The results showed a significant decrease in the mean minimum diameter fiber stimulated for electrodes that encircled the nerve up to θ = 330°. The results for the longer electrodes were fairly similar to those without the narrowed electrode in that the overlapping resulted in a decrease in stimulation. The activation pattern in the individual models was similar to those in Figures 2 and 3.

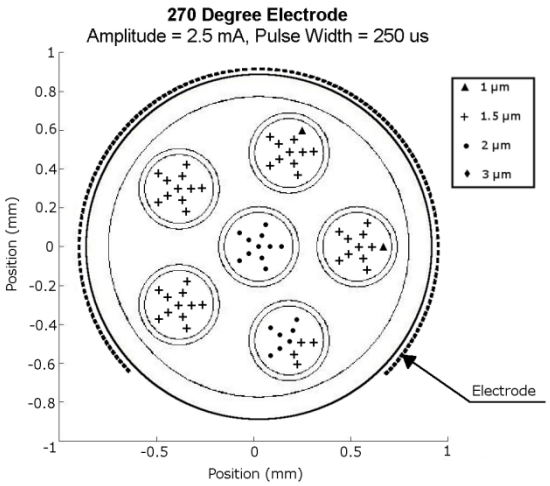

Fig. 2. The smallest fiber stimulated at each of the 66 tested locations using a θ=270° electrode.

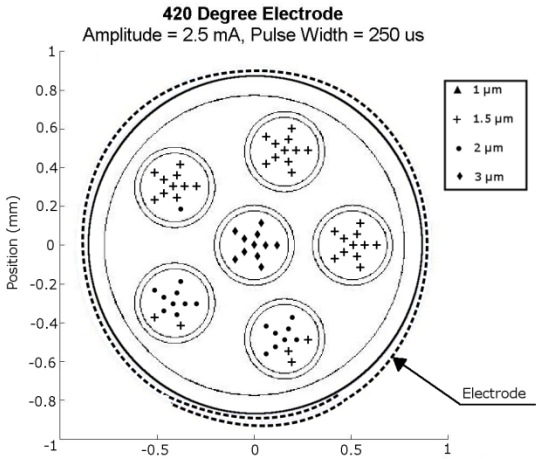

Fig. 3. The smallest fiber stimulated at each of the 66 tested locations using a θ=420° electrode.

IV. Discussion

The decrease in stimulation near the electrode ends, or the area where the ends of the electrode ends overlap radially, can be explained through interpretation of the activating function. Upon substituting Equation (5) for the axoplasm conductance in the activating function, Equation (3), yields (8), which is the second spatial difference in voltage along the longitudinal axis of the nerve. When $L \to 0$, (8) becomes the second spatial derivative of voltage with respect to the longitudinal axis of the nerve, and is related to how abruptly the voltage changes in the longitudinal direction. Therefore, in order to maximize stimulation, the longitudinal change in voltage must be highly concentrated.

$$I(n,t) = \frac{\pi d^2 \left[V_e(n-1,t) - 2V_e(n,t) + V_e(n+1,t) \right]}{4\rho_a L} \tag{8}$$

In the cases where θ < 360°, most of the field in the areas of the nerve far from the overlap area, is caused by current flowing out of the nearest portions of the electrode, and the change in the field is fairly concentrated along the longitudinal axis of the nerve. However, near the area of overlap, each electrode end creates a distinct field. These two fields overlap, and because of the pitch of the electrode, they are longitudinally offset from each other along the axis of the nerve. The overlapping fields and the offset of the electrode ends, cause the longitudinal change in voltage to become less concentrated near the area of overlap. This phenomenon is illustrated in Figure 4. Further evidence of the decreased concentration of the change in voltage can be seen in models where θ > 360°. As the electrode continues to overlap radially, the two fields created by these overlapping sections combine, resulting in less stimulation of the neurons near those areas.

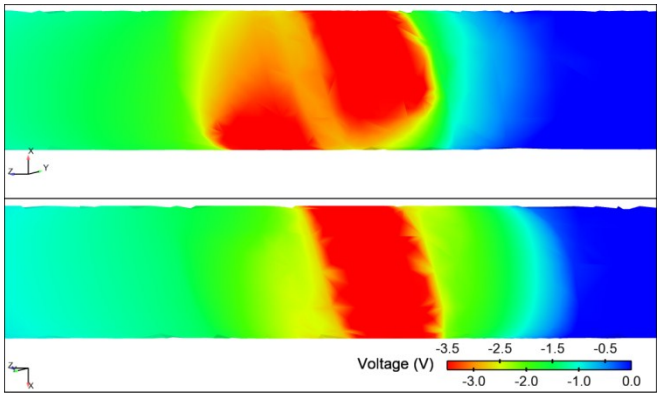

Fig. 4. An ANSYS calculated voltage on the outer surface of the nerve created by a 330° helical electrode. Top, the voltage distribution created by the electrode ends. Bottom, the voltage distribution near the middle of the electrode, far from the electrode ends.

V. Conclusion

While increasing the length of the electrode in each set of models resulted in decreased stimulation, some improvements to the design of helical electrodes are apparent. In order to improve the uniform stimulation of fibers within a nerve bundle, design improvements should focus on concentrating the longitudinal change in voltage distribution near the electrode ends. One simple improvement would be to decrease the pitch of the electrode so the longitudinal offset between the electrode ends is minimized.

Tapering the ends of the electrodes might also be effective in preventing a decrease in stimulation at the area of overlap. By tapering each of the electrode ends toward the longitudinal center of the helix, on an electrode that extends close to 360°, the axial distance between the extreme longitudinal edges of the electrode ends is reduced. The taper will reduce the axial length of the field created by each of the smaller electrode ends. The two fields will still overlap, but the longitudinal extent of the field should be reduced, leading to a more concentrated change in voltage. Because high current concentrations tend to form near sharp angles, the ends of the tapered electrodes may need to be rounded or flattened. Additionally, tapering the ends of the electrode away from the longitudinal center of the helix, or increasing the electrode pitch, may prevent the fields from overlapping and create two distinct, concentrated, fields at each electrode end.

References

[1] W. F. M. Agnew, D.B. and Yuen, T.G.H., "Principles for safe and effective nerve stimulation," in *New Pespectives in Sacral Nerve Stimulation: For Control of Lower Urinary Tract Dysfunction* U. G. Jonas, Volker, Ed., ed London: Martin Dunitz, Ltd., 2002, pp. 29-40.

[2] A. Q. Choi*, et al.*, "Selectivity of multiple-contact nerve cuff electrodes: a simulation analysis," *IEEE Trans Biomed Eng,* vol. 48, pp. 165-72, Feb 2001.

[3] R. Plonsey and D. B. Heppner, "Considerations of quasi-stationarity in electrophysiological systems," *Bull Math Biophys,* vol. 29, pp. 657-64, 1967 1967.

[4] W. M. Grill and J. T. Mortimer, "Electrical properties of implant encapsulation tissue," *Annals of Biomedical Engineering,* vol. 22, pp. 23-33, 1994 1994.

[5] T. A. Frieswijk*, et al.*, "Force-current relationships in intraneural stimulation: Role of extraneural medium and motor fibre clustering," *Medical and Biological Engineering and Computing,* vol. 36, pp. 422-430, July 1998.

[6] E. V. Goodall*, et al.*, "Modeling study of activation and propagation delays during stimulation of peripheral nerve fibers with a tripolar cuff electrode," *IEEE Transactions on Rehabilitation Engineering,* vol. 3, pp. 272-282, 09 1995.

[7] D. R. McNeal, "Analysis of a model for excitation of myelinated nerve," *IEEE Trans Biomed Eng,* vol. 23, pp. 329-37, 1976 1976.

[8] E. N. Warman*, et al.*, "Modeling the effects of electric fields on nerve fibers: determination of excitation thresholds," *IEEE Trans Biomed Eng,* vol. 39, pp. 1244-54, 1992 1992.

[9] J. D. Sweeney*, et al.*, "A nerve cuff technique for selective motor control," in *Proceedings of the Annual International Conference of the IEEE Engineering in Medicine and Biology Society (IEEE Cat. No.88CH2566-8)*, New Orleans, LA,, 1988, pp. 1517-18 vol.4.

[10] R. B. Szlavik and H. de Bruin, "The effect of stimulus current pulse width on nerve fiber size recruitment patterns," *Medical Engineering and Physics,* vol. 21, pp. 507-515, July-Sept. 1999.